

Phase lag variability associated with the 1–10 Hz QPO in GRS 1915+105

P. Reig^{1,2}, T. Belloni³, M. van der Klis⁴, M. Méndez^{4,5}, N. Kylafis^{1,2}, E. C. Ford⁴

ABSTRACT

We have used *Rossi X-ray Timing Explorer* data to measure the lags between soft (2–5 keV) and hard (5–13 keV) photons and to study the aperiodic variability of the superluminal black hole candidate GRS 1915+105 during low-flux states. The power density spectra exhibit quasi-periodic oscillations (QPO) whose frequency increases with increasing count rate and varies in the frequency range 0.6–8 Hz. A correlation between the QPO frequency and the phase lag spectra is reported for the first time. This correlation is found for both the phase lag continuum and the phase lag at the QPO frequency, although the shape of the correlations is somewhat different. We find that as the QPO frequency moves to higher values the phase lags reverse sign from positive to negative. The absolute value of the lag always increases with photon energy. The negative (soft) lags are associated with a softer energy spectrum, whereas the positive (hard) lags are seen when the source is harder. We describe two different scenarios that may account for the change in the sign of the lags.

Subject headings: accretion — accretion disks — stars: neutron — stars: individual (GRS 1915 +105) — X-rays: stars

¹Foundation for Research and Technology-Hellas, 711 10 Heraklion, Crete, Greece

²Physics Department, University of Crete, 710 03 Heraklion, Crete, Greece

³Osservatorio Astronomico di Brera, Via E. Bianchi 46, I-23807 Merate (LC), Italy

⁴Astronomical Institute “Anton Pannekoek”, University of Amsterdam and Center for High-Energy Astrophysics, Kruislaan 403, NL-1098 SJ Amsterdam, the Netherlands

⁵Facultad de Ciencias Astronómicas y Geofísicas, Universidad Nacional de La Plata, paseo del Bosque S/N, 1900 La Plata, Argentina

1. Introduction

The X-ray source GRS 1915+105 was discovered in 1992 with the WATCH instrument onboard GRANAT (Castro-Tirado et al. 1992). Since RXTE established continuous coverage in 1996 February, GRS 1915+105 has never switched off completely. It was the first galactic object to show superluminal radio expansion (Mirabel & Rodríguez 1994). It is located at a distance between 6 to 12.5 kpc (Mirabel & Rodríguez 1994; Fender et al. 1999). Due to high extinction in the line of sight no optical study of GRS 1915+105 has been possible and only an infrared counterpart has been suggested (Mirabel et al. 1994). No binary mass function or orbital period are known.

The source is believed to host a black hole on the basis of its similarities to the dynamically proven black hole system GRO 1655–40 (Orosz & Bailyn 1997) and its X-ray luminosity, which is above the Eddington limit for a neutron star. The X-ray spectrum of GRS 1915+105 is also typical of black hole candidates, requiring two main components (Belloni et al. 1997a): a power-law component which accounts for the high energy part of the spectrum and a thermal component (multi-color black body) which dominates at energies below 10 keV (Mitsuda et al. 1984). At times only the power law component is observed (Trudolyubov, Churazov, & Gilfanov 1999; Belloni et al. 2000).

GRS 1915+105 displays a remarkable richness in variability (see e.g. Greiner, Morgan & Remillard 1997). Belloni et al. (1997a,b) modeled the main type of variations observed in this source as due to the onset of a thermal-viscous instability. In this framework, the intervals of low flux correspond to the non-observability of the innermost portion of the accretion disk. During three long (30–100 days) periods in 1996 and 1997, no strong flux variability was observed from GRS 1915+105. On the basis of an X-ray color analysis of the RXTE/PCA data, Belloni et al. (2000) interpreted these quiet periods as the result of the recovery from an instability that affected a larger portion of the accretion disk, combined with a relatively lower value of the accretion rate. Detailed timing analysis of part of these observations has been presented by Trudolyubov et al. (1999).

Three different types of QPO have been identified in GRS 1915+105 (Morgan, Remillard & Greiner 1997). At higher frequencies a sharp ($Q \approx 20$) QPO with constant centroid frequency at 67 Hz and whose

rms amplitude increases with photon energy has been detected. This QPO has been proposed to arise in the inner accretion disk and its frequency is thought to reflect the properties of the black hole. At much lower frequencies (0.001–0.1 Hz), the source occasionally shows high-amplitude QPO or brightness “spatters”. These variations probably correspond to a disk instability. The third class of QPO observed in GRS 1915+105 comprises those detected in the frequency range 0.5–10 Hz. They are linked to the properties of the accretion disk since their centroid frequency and fractional rms have been reported to correlate with the thermal flux (Markwardt, Swank, & Taam 1999; Trudolyubov et al. 1999) and apparent temperature (Muno, Morgan, & Remillard 1999) of the disk. These QPO are observed only during the low-flux intervals when, according to the model of the thermal-viscous instability, a portion of the inner accretion disk is not observable.

A phase-lag analysis of the observation which showed the strongest signal at 67 Hz was presented by Cui (1999): the 67 Hz QPO shows a marked hard lag, while the low frequency (well below 1 Hz) QPO shows a complex hard/soft lag structure.

In this paper, we concentrate on the phase lags associated with the properties of the 0.5–10 Hz QPO during two of the long quiet intervals mentioned above.

2. Observations

The data used in this work were retrieved from the public *RXTE* archive and correspond to two different sets of observations. The first set took place between 1996 July 11 and 1996 August 18 and consists of 27 pointings. The second set comprises 15 observations covering the period between 1997 September 29 and 1997 November 24. The two sets of observations correspond to low-flux intervals in which the source did not display structured variability either in the PCA or in the ASM data (Belloni et al. 2000). The journal of the *RXTE* observations is given in Table 1. Due to its low-Earth orbit, *RXTE* data consist of a number of contiguous data intervals (typically 1.5–3 hour long) interspersed with observational gaps produced by Earth occultations of the source and passages of the satellite through the South Atlantic Anomaly. These intervals were analysed separately and appear as different “observations” in Table 1. A suffix *a, b, c, ...* has been added to the data set identifiers accordingly.

3. Analysis and Results

3.1. Noise components in the power density spectrum

In order to study the source variability in the 0.5–20 Hz range, we divided the 2–60 keV PCA light curves (no energy selection was made) of each observation into 16 s segments and calculated the Fourier power spectrum of each segment. The Nyquist frequency was 256 Hz for the first set of observations and 64 Hz for the second. The contribution by the photon counting noise was computed and subtracted from each power spectrum. The power spectra were normalized such that their integral gives the squared fractional rms variability (Belloni & Hasinger 1990). The power spectra were then averaged together to produce one power spectrum for each observation.

In all power spectra a strong band-limited noise component was present, together with one or more QPO peaks. We fitted the power spectra using a model that consisted of a broken power law and two Lorentzian peaks, representing the band-limited noise continuum and the QPO plus its second harmonic, respectively. While all power spectra clearly showed one QPO peak, in some cases the second harmonic was not required. Generally, the power spectra are characterized by a flat power-law below the QPO frequency ($\alpha=0.1-0.3$) and a steep power-law above the QPO ($\alpha=2.7-3.0$). The slope of the low-frequency power-law tends to increase with increasing QPO frequency. While the QPO frequency increases with count rate, its amplitude (rms) decreases (Fig 1). Trudolyubov et al. (1999) found the same trend during the 1996 November–1997 April low-flux period. The results of the power spectral fitting are given in Table 1.

3.2. Phase lags

For each observation, we produced a phase-lag spectrum. We divided the data into two energy bands (soft: 2–5 keV; hard: 5–13 keV) and produced a cross spectrum for every 16 s. The cross spectrum is defined as $C(j) = X_1(j) \cdot X_2(j)$, where X_1 and X_2 are the complex Fourier coefficients for the two energy bands at a frequency ν_j , and $X_1(j)^*$ is the complex conjugate of $X_1(j)$ (van der Klis et al. 1987). The phase lag between the signals in the two bands at Fourier frequency ν_j is $\phi_j = \arg[C(j)]$ (the position angle of $C(j)$ in the complex plane) and the corresponding time lag $\phi_j/2\pi\nu_j$. We calculated an average

cross vector C by averaging the complex values over multiple 16 s spectra and binning in frequency, and then finding the final value of ϕ vs. frequency. The error in ϕ is computed from the observed variance of C in the real and imaginary directions. We limited our analysis to frequencies below 10 Hz, well below the region where binning effects are important (Crary et al. 1998). In all phase lag spectra, positive lag values mean that hard photons are lagging soft photons. No correction for dead-time effects in the phase lag spectra (cross-talk between energy channels) were done since this effect was found to be negligible.

In order to study the variability of the phase lags and its relationship with the properties of the QPO we obtained the mean phase lag spectrum by averaging the cross-correlation vectors in four different QPO frequency ranges, $\nu_{QPO} < 1$ Hz, $1 \leq \nu_{QPO} < 2$ Hz, $2 \leq \nu_{QPO} < 3$ Hz and $\nu_{QPO} \geq 3$ Hz. Figure 2 shows these four phase lag spectra together with a representative power spectrum of the group. One can see that both the lag at the QPO frequency, and the characteristic shape of the lag continuum vary drastically. A common feature of the lag spectra is the presence of a broad dip at around the QPO frequency. As the QPO frequency increases, its position in the dip changes. The dip itself also increases with frequency but not as fast. The value of the QPO frequency falls below the dip minimum when it is low and around the dip minimum when it takes intermediate and high values.

At low values of the QPO frequency, the power of the continuum below 1 Hz increases with frequency and the phase lag of the continuum is positive whereas at high and intermediate QPO frequencies the continuum is flatter and close to zero lag. Averaging over the 0.06–0.6 Hz range, that is, below any of the QPOs, for the four cases shown in Figure 2 we find the following values of the phase lags: 0.215 ± 0.004 rad for $\nu_{QPO} < 1$ Hz, 0.159 ± 0.004 rad for $1 \leq \nu_{QPO} < 2$ Hz, 0.071 ± 0.004 rad for $2 \leq \nu_{QPO} < 3$ Hz and -0.024 ± 0.003 rad for $\nu_{QPO} \geq 3$ Hz.

We also derived phase lags of the continuum and at the QPO frequency for each observation, by measuring the average vector in the frequency range $0.1-5$ Hz and $\nu_{QPO} \pm \frac{1}{2}\Delta\nu$, respectively. $\Delta\nu$ is the FWHM of the QPO peak. The results were plotted as a function of QPO frequency and are shown in Figure 3. A tight correlation between these quantities is found. As the QPO frequency increases the lag decreases, changing sign at around 2 Hz. The increase above 5 Hz observed in Figure 3 (bottom) is due to the dip

moving toward higher frequencies. This change in the sign of the lag means that at a certain point soft photons lag hard photons. Similar results were obtained for the lags measured at the theoretical harmonics of the QPO frequency. Although, at most, only one harmonic is seen in the power spectra, we produced phase lags versus frequency plots at 2, 3 and 4 times the QPO frequency. These plots showed the same trend as when the QPO frequency is used. The frequency at which the lags change from positive to negative are consistent with 4, 6 and 8 Hz, that is, 2, 3 and 4 times that of the QPO (2 Hz).

In Figure 4, the dependence of the phase lags (at the QPO frequency) on energy is plotted. Different symbols correspond to three different values of the QPO frequency: squares for $\nu_{QPO}=0.999$ Hz, dots for $\nu_{QPO}=2.316$ Hz and stars for $\nu_{QPO}=4.68$ Hz. The energy bands shown are 2.0–5.0, 5.4–6.9, 7.2–9.4 and 9.8–13.1 keV. The phase lag was obtained by taking the softest band as the reference band and by computing a cross-power spectrum between each of the energy bands and the reference band. At low frequencies, the phase lags are positive and increase with energy; at high frequencies the phase lags are negative and decrease with energy; at intermediate frequencies the lags are zero and roughly constant.

We also calculated background subtracted light curves corresponding to the following bands in pulse-height channels: 0–13 (2.0–5.0 keV, band A), 14–35 (5.0–13.0 keV, band B) and 36–100 (13.0–60.0 keV, band C) and produced hard and soft colors as $HR1 = B/A$ and $HR2 = C/A$, respectively. In Figure 5 we plot phase lags of the continuum (0.1–5 Hz) as a function of $HR1$. The negative lags occur when the source is softer ($HR1 \lesssim 1.2$), whereas the hard lags are seen when the source spectrum is harder ($HR1 \gtrsim 1.3$). A similar trend is obtained if the hard color $HR2$ is used. For an interpretation of X-ray colors in terms of spectral models, see Belloni et al. (2000).

4. Discussion

We have analysed RXTE data of the superluminal source GRS 1915+105 when it was in quiescence. This state is characterized by a 0.5–10 Hz QPO which shifts in frequency in correlation with the count rate and the hardness ratios. We have measured lags of the 5–13 keV photons relative to the 2–5 keV and found that both positive and negative lags are present. The sign of the phase lags changes as the QPO central fre-

quency crosses 2 Hz. Also, negative lags occur when the energy spectrum is soft ($HR1 < 1.3$).

Belloni et al. (1997a,b) have shown that the complex spectral and temporal variability of GRS 1915+105 can be explained by the rapid removal and subsequent refilling of the inner region of the accretion disk. The quiescent state corresponds to the absence of this inner region and it is characterized by a hard spectrum and the presence of 0.5–10 Hz QPO. The changes of the QPO centroid frequency are strongly correlated with the changes of spectral and other timing parameters. We note that the 0.5–10 Hz QPO are present only when the X-ray flux is low and the spectrum is hard, the ‘C’ state in Belloni et al. (2000). Steady high-luminosity soft states do not contain 0.5–10 Hz QPO (Muno et al. 1999).

The properties of the QPO parameters can be summarized as follows. As the frequency of the QPO increases *i)* the flux of the soft component (disk) increases (Markwardt et al. 1999), *ii)* the temperature of the accretion disk increases (Muno et al. 1999), *iii)* the fractional rms amplitude of the QPO decreases (Trudolyubov et al. 1999). In this work we find that *iv)* as the frequency of the QPO increases the lag between hard and soft photons decreases, changing sign for $\nu_{QPO} \gtrsim 2$ Hz (Fig. 3), *v)* negative lags occur when the power-law spectrum is soft and positive lags when it is hard (Fig. 5), *vi)* the 0.5–10 Hz QPO disappears when the PCA intensity is high ($\gtrsim 21000$ counts per second).

The X-ray spectra of black hole systems consist of a power-law component plus a soft thermal component. The relative strength of these components varies with X-ray flux in the 1–10 keV band. When the X-ray spectrum is dominated by the power-law component, we expect the inverse Compton scattering to be in action. Therefore, we expect that the hard photons lag the soft photons, i.e., positive lags. One possible explanation for the soft lags is that the photons that give rise to such lags come from the disk (soft) component. The soft photons from this disk component will not be delayed with respect to the hard photons because, unlike the power-law photons, a large fraction of them are not produced by Comptonization. Thus, no or small delays are expected. More difficult to explain are the negative lags. They may be due to direct Compton scattering if the soft photons are energetic enough.

The above scenario requires that a large fraction of the soft photons escape unscattered. This seems

difficult to reconcile with the power-law dominated spectra that characterized our observations. Alternatively, we may think of a Comptonizing region in which the Comptonization process becomes more efficient closer to the black hole. The soft photons are first up-scattered by collisions with fast-moving and/or hot electrons and in doing so they travel around the Comptonizing region. Some of these photons escape and produce the power-law and the hard lags. But some fraction of these hard photons find themselves in the outer parts of the Comptonizing region where the velocity and/or temperature of the electrons is low and they begin to give energy by means of the normal Compton effect. The downward scattering would originate the soft (negative) lags. In order for such downward scattering to occur the optical depth must be high, so that the photons sample a large fraction of the Comptonizing medium. If the optical depth is low the photon escapes after few scatterings. Since the photon energy is much lower than that of the electrons only upscattering would occur. One such physical situation would be, for example, a disk with a Keplerian distribution of velocities (Reig, Kylafis & Spruit 2000). Near the black hole the rotational velocity, is close to the speed of light and the photons suffer bulk Comptonization, i.e., inverse Compton scattering. Far enough from the black hole the velocity is too low and the reverse process, i.e. direct Compton scattering, takes on.

This work was supported by the Netherlands Foundation for research in astronomy (ASTRON) under grant 781-76-017, by the Netherlands Research School for Astronomy (NOVA), and the NWO Spinoza grant 08-0 to E.P.J. van den Heuvel. PR acknowledges support from the European Union through the Training and Mobility Research Network Grant ERBFMRX/CT98/0195. This research has made use of data obtained through the High Energy Astrophysics Science Archive Research Center Online Service, provided by the NASA/Goddard Space Flight Center.

REFERENCES

- Belloni T. & Hainger G., 1990, A&A, 230, 103
- Belloni T., Méndez M., King A.R., van der Klis M. & van Paradijs J., 1997a, ApJ, 479, L145
- Belloni T., Méndez M., King A.R., van der Klis M. & van Paradijs J., 1997b, ApJ, 488, L112
- Belloni T., Klein-Wolt, M., Méndez M., van der Klis M. & van Paradijs, 2000, A&A, submitted
- Castro-Tirado, A.J., Brandt S. & Lund N., 1992, IAU Circ., 5590
- Crary, D. J.; Finger, M. H., Kouveliotou, c., van der Hooft, F., van der Klis, M., Lewin, W. H. G. & van Paradijs, J. 1998, ApJ, 493, L71
- Cui W., 1999, ApJ, 524, L59.
- Fender, R. P.; Garrington, S. T., McKay, D. J., Muxlow, T. W. B., Pooley, G. G., Spencer, R. E., Stirling, A. M. & Waltman, E. B., 1999, MNRAS, 304, 865
- Greiner J., Morgan E.H. & Remillard R.A., 1997, ApJ, 473, L107
- Liang E.P., Physics Reports, 302, 67
- Morgan E.H., Remillard R.A. & Greiner J., 1997, ApJ, 482, 993
- Markwardt C.B., Swank J.H. & Taam R.E., 1999, ApJ, 513, L37
- Mirabel, I. F.; Duc, P. A., Rodriguez, P. A., Teyssier, R., Paul, J., Claret, A., Auriere, M., Golombek, D. & Marti, J., 1994, A&A, 282, L17
- Mirabel F. & Rodríguez L., 1994, Nature, 371, 46
- Mitsuda K, Inoue H., Koyama K., et al., 1984, PASJ, 36, 741
- Muno M. P., Morgan E. H. & Remillard R. A., 1999, astro-ph/9904087
- Orosz J.A. & Bailyn C.D., 1997, ApJ, 477, 876
- Reig P., Kylafis N. & Spruit, 2000, in preparation
- Trudolyunov S., Churazov E. & Gilfanov M., 1999, astro-ph/9811449
- van der Klis, M., Hasinger, G., Stella, L., Langmeier, A., van Paradijs, J. & Lewin, W. H. G., 1987, ApJ, 319, L13

TABLE 1
RXTE OBSERVATIONS OF GRS 1915+105

Observation ID	MJD	PCA (c/s)	ν_{QPO} (Hz)	rms (%) (0.01-20 Hz)	rms (%) (QPO)	lag (rad) at ν_{QPO}	time lag (ms)
1996 July 11 – August 18							
10408-01-22-00a	50275.0905	9778.3	3.468±0.011	9.58±0.15	9.17±0.25	-0.082±0.015	-3.8±0.7
10408-01-22-00b	50275.1072	9789.0	3.475±0.005	11.09±0.07	9.31 ±0.15	-0.096±0.009	-4.4±0.4
10408-01-22-01	50275.2238	9282.4	2.768±0.006	10.45±0.10	10.68 ±0.13	-0.045±0.006	-2.6±0.3
10408-01-22-02a	50275.3572	9008.1	2.561±0.005	10.45±0.09	11.39±0.12	-0.027±0.006	-1.7±0.4
10408-01-22-02b	50275.4238	9175.3	2.840±0.023	9.31±0.10	9.96±0.87	-0.032±0.034	-1.8±1.9
10408-01-23-00a	50278.4921	9735.2	3.480±0.004	9.87±0.08	10.27±0.12	-0.098±0.007	-4.5±0.3
10408-01-23-00b	50278.5585	9709.6	3.614±0.005	10.20±0.07	9.90±0.11	-0.103±0.006	-4.6±0.3
10408-01-23-00c	50278.6266	10457.7	4.209±0.009	9.65±0.08	9.12±0.11	-0.122±0.006	-4.6±0.2
10408-01-24-00a	50280.1702	8923.9	2.238±0.005	11.45±0.10	12.13±0.11	-0.001±0.006	-0.1±0.4
10408-01-24-00b	50280.2266	8900.8	2.316±0.005	10.95±0.12	12.00±0.16	0.001±0.005	0.1±0.4
10408-01-24-00c	50280.2933	8955.6	2.537±0.004	11.62±0.15	11.34±0.15	-0.036±0.006	-2.3±0.4
10408-01-24-00d	50280.3599	9011.1	2.598±0.008	10.68±0.15	10.95±0.28	-0.055±0.011	-3.3±0.7
10408-01-25-00a	50283.4947	8263.6	1.110±0.003	12.92±0.11	11.67±0.20	0.172±0.007	24.7±1.0
10408-01-25-00b	50283.5620	8154.0	1.077±0.003	13.06±0.10	11.24±0.21	0.185±0.007	27.3±1.0
10408-01-25-00c	50283.6286	8076.9	1.184±0.002	12.28±0.14	12.06±0.16	0.154±0.006	20.6±0.8
10408-01-27-00a	50290.5774	7887.2	0.644±0.002	13.73±0.11	9.74±0.28	0.247±0.014	72.7±4.1
10408-01-27-00b	50290.6322	7925.8	0.621±0.003	13.12±0.12	9.66±0.22	0.285±0.010	73.0±2.7
10408-01-27-00c	50290.6988	7826.5	0.629±0.003	13.04±0.20	10.28±0.19	0.272±0.008	68.9±2.1
10408-01-28-00a	50298.5696	7751.1	0.999±0.003	12.33±0.11	11.36±0.18	0.189±0.006	30.0±1.0
10408-01-28-00b	50298.6362	7755.6	0.962±0.003	13.49±0.12	11.21±0.21	0.201±0.007	33.3±1.2
10408-01-28-00c	50298.7029	7533.5	0.928±0.003	13.16±0.13	11.55±0.19	0.221±0.007	38.0±1.2
10408-01-29-00a	50305.3736	7951.5	1.673±0.004	12.51±0.13	11.98±0.17	0.085±0.007	8.1±0.6
10408-01-29-00b	50305.4398	8070.8	1.858±0.004	12.15±0.11	11.97±0.16	0.049±0.005	4.2±0.5
10408-01-29-00c	50305.5064	8078.7	1.962±0.003	12.16±0.11	11.95±0.15	0.036±0.005	3.0±0.4
10408-01-30-00a	50313.3135	11560.3	4.551±0.009	8.75±0.10	8.95±0.08	-0.140±0.006	-4.9±0.2
10408-01-30-00b	50313.3801	12979.6	5.030±0.008	10.85±0.08	7.26±0.22	-0.171±0.006	-5.4±0.2
10408-01-30-00c	50313.4468	14701.7	5.551±0.015	13.21±0.13	4.72±0.18	-0.188±0.008	-5.4±0.2
1997 September 29 –October 25							
20402-01-48-00a	50720.5910	21914.4	7.56 ±0.03	18.09±0.15	2.50 ±0.06	-0.260±0.011	-5.5±0.2
20402-01-48-00b	50720.6572	12618.6	4.68 ±0.01	11.83±0.06	5.62 ±0.09	-0.147±0.008	-5.0±0.3
20402-01-48-00c	50720.6783	11805.7	4.54±0.04	11.45±0.20	7.14±0.29	-0.179±0.022	-6.3±0.8
20402-01-49-00a	50729.3275	8714.6	2.911±0.005	10.18±0.07	10.89±0.11	-0.033±0.006	-1.8±0.3
20402-01-49-00b	50729.3940	8369.3	2.621±0.006	10.60±0.10	11.05±0.16	-0.015±0.007	-0.9±0.4
20402-01-49-01	50730.3949	8197.8	2.721±0.005	10.76±0.07	10.96±0.12	-0.041±0.006	-2.4±0.3
20402-01-50-00	50735.5474	6579.2	0.844±0.003	13.51±0.18	10.52±0.29	0.239±0.010	45.0±2.0
20402-01-50-01a	50737.4047	6607.5	1.016±0.003	13.76±0.11	10.82±0.21	0.201±0.009	31.5±1.3
20402-01-50-01b	50737.4766	6373.4	1.079±0.003	13.60±0.14	11.09±0.22	0.189±0.010	27.8±1.4
20402-01-51-00a	50743.2947	6626.3	1.399±0.006	13.92±0.17	11.71±0.31	0.130±0.012	14.7±1.3
20402-01-51-00b	50743.3377	6602.3	1.355±0.004	13.73±0.12	11.60±0.20	0.135±0.007	15.9±0.8
20402-01-51-00c	50743.4092	6584.0	1.399±0.005	13.84±0.13	11.38±0.20	0.133±0.007	15.1±0.8
20402-01-51-00d	50743.4801	6640.4	1.442±0.003	13.55±0.14	11.97±0.20	0.116±0.008	12.8±0.9
20402-01-52-00a	50746.5509	6657.3	1.413±0.005	13.77±0.12	11.27±0.22	0.134±0.009	15.2±1.1
20402-01-52-00b	50746.6190	6667.5	1.482±0.005	13.86±0.14	11.89±0.24	0.149±0.010	16.1±1.1
20402-01-52-00c	50746.6898	6767.9	1.602±0.004	12.90±0.18	11.86±0.27	0.083±0.010	8.3±1.0

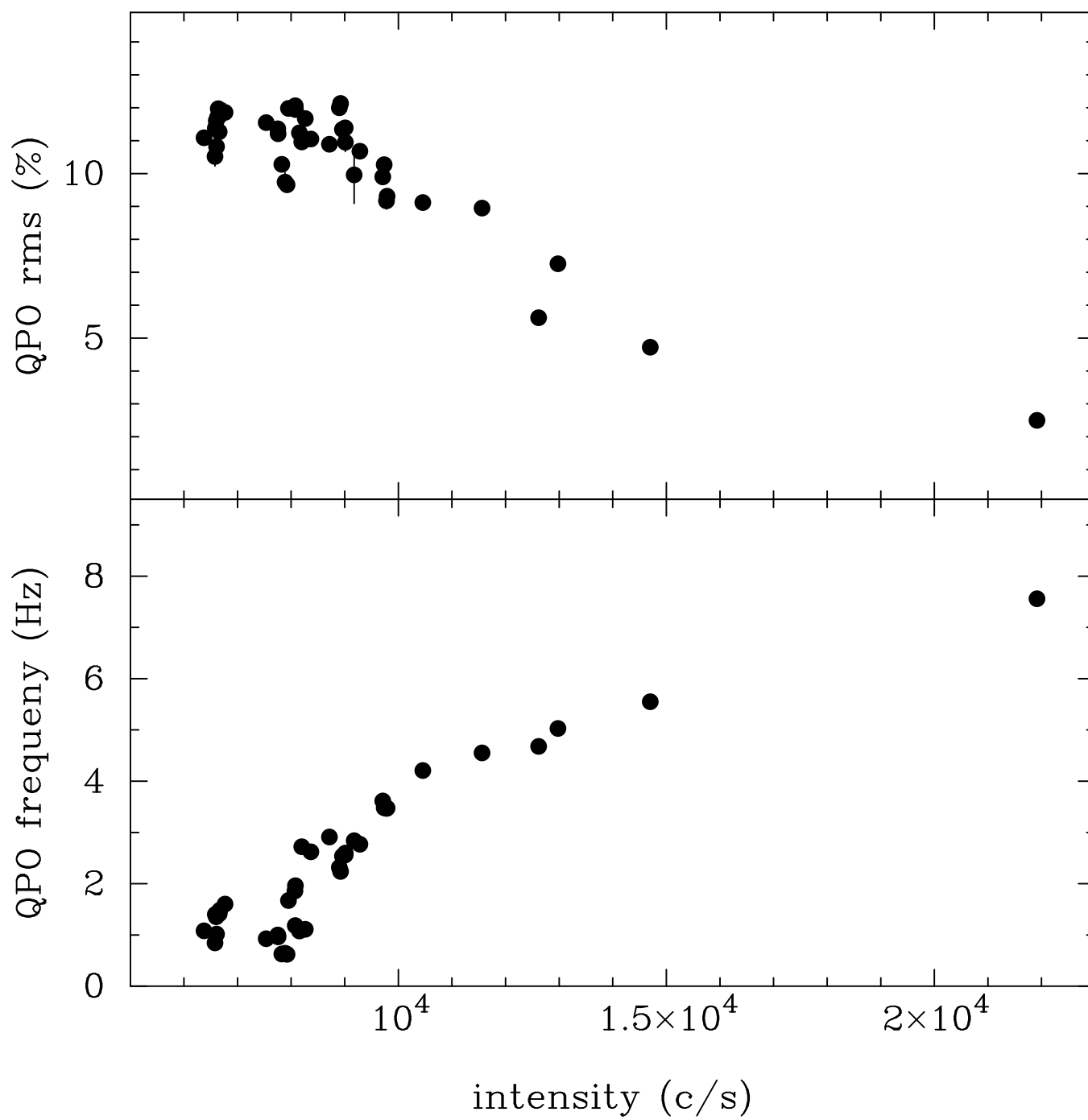
Fig. 1.— Variation of the *rms* amplitude and frequency of the QPO with count rate.

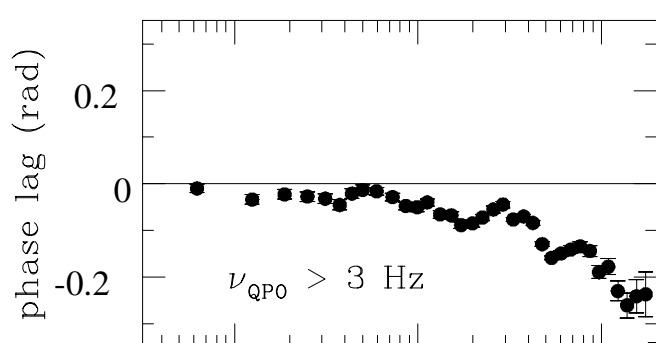
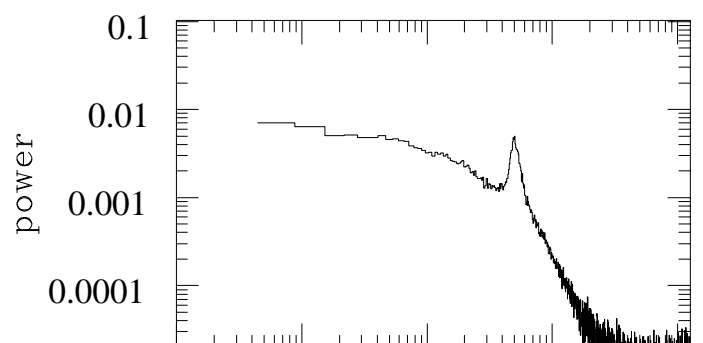
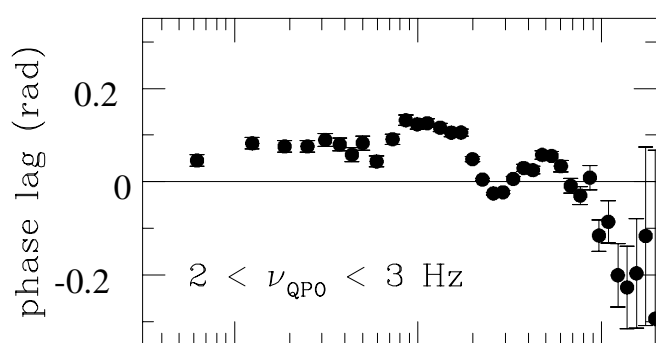
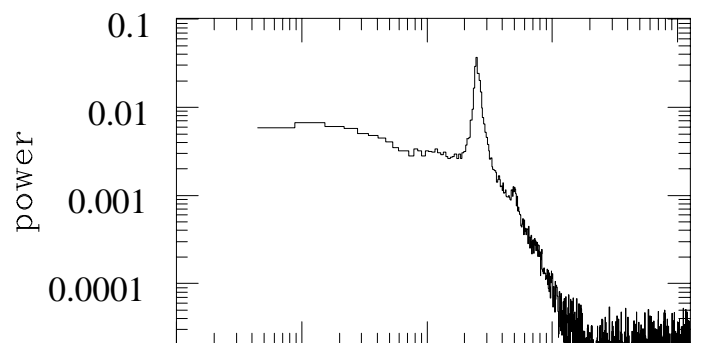
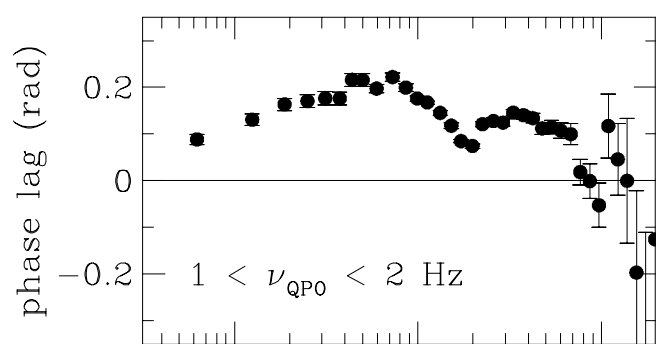
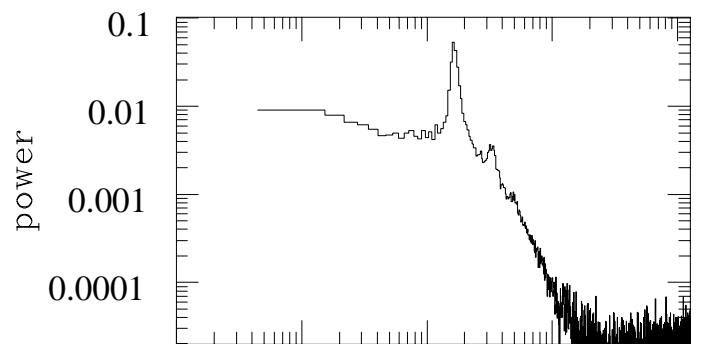
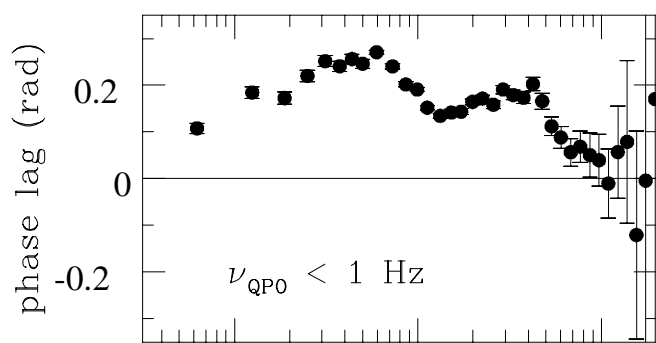
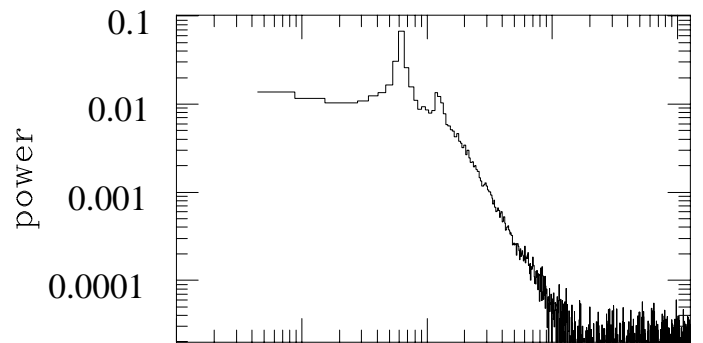
Fig. 2.— Power and phase lag spectra versus Fourier frequency for four QPO frequency ranges. The phase lag spectra are the average of all those included in the frequency range shown. The power spectra are individual examples of a representative member of the group. Positive lags means that hard photons lag soft photons.

Fig. 3.— Phase lag at the QPO frequency (top panel) and phase lag of the continuum in the frequency range 0.1–5 Hz (bottom panel) versus QPO frequency. Different symbols represent different observing runs as follows: 1996 July 11 – August 18 (circles), 1997 September 29 –October 25 (stars)

Fig. 4.— Dependence of the lags (at QPO frequency) on energy. Different symbols correspond to three different values of the QPO frequency: squares for $\nu_{QPO}=0.999$ Hz, dots for $\nu_{QPO}=2.316$ Hz and stars for $\nu_{QPO}=4.68$ Hz. The lags were calculated between the energy bands 4.6–5.9 keV, 6.2–8.1 keV and 8.4–10.9 keV with respect to the soft band 2.0–4.3 keV.

Fig. 5.— Phase lags as a function of the soft color HR1=5–13 keV/2–5 keV. Negative lags are seen only when the source is soft.





0.01 0.1 1 10 100
Frequency (Hz)

0.1 1 10
Frequency (Hz)

